# Design and Kinematic Optimization of a Two Degrees-of-Freedom Planar Remote Center of Motion Mechanism for Minimally Invasive Surgery Manipulators

**Sajid Nisar**[1]
Mechatronics Laboratory,
Mechanical Engineering and Science,
Kyoto University,
Kyoto 615-8540, Japan
e-mail: nisar.sajid.78v@kyoto-u.jp

**Takahiro Endo**
Department of Mechanical Engineering
and Science,
Kyoto University,
Kyoto 615-8540, Japan
e-mail: endo@me.kyoto-u.ac.jp

**Fumitoshi Matsuno**
Department of Mechanical Engineering
and Science,
Kyoto University,
Kyoto 615-8540, Japan
e-mail: matsuno@me.kyoto-u.ac.jp

*Minimally invasive surgery (MIS) requires four degrees-of-freedom (DOFs) (pitch, translation, yaw, and roll) at the incision point, but the widely used planar remote center of motion (RCM) mechanisms only provide one degree-of-freedom. The remaining three DOFs are achieved through external means (such as cable-pulleys or actuators mounted directly on the distal-end) which adversely affect the performance and design complexity of a surgical manipulator. This paper presents a new RCM mechanism which provides the two most important DOFs (pitch and translation) by virtue of its mechanical design. Kinematics of the new mechanism is developed and its singularities are analyzed. To achieve maximum performance in the desired workspace region, an optimal configuration is also evaluated. The design is optimized to yield maximum manipulability and tool translation with smallest size of the mechanism. Unlike the traditional planar RCM mechanisms, the proposed design does not rely on external means to achieve translation DOF, and therefore, offers potential advantages. The mechanism can be a suitable choice for surgical applications demanding a compact distal-end or requiring multiple manipulators to operate in close proximity.* [DOI: 10.1115/1.4035991]

## 1 Introduction

Minimally invasive surgery is a well-known surgical technique which offers numerous advantages over the traditional open surgery methods. Less blood-loss, quicker postoperation recovery, and shorter bed stay make it more efficacious and cost effective [1–4]. Due to multiple advantages of MIS over open surgery [5], it is being widely practiced in the modern-day operation theaters [6,7].

However, MIS is a difficult to perform surgical technique [8] as it requires highly controlled tool movements inside the patient body [9–12]. To overcome this difficulty, robotic manipulators have become a natural choice as their precision performance is already well established [13]. A number of surgical manipulators have been proposed and developed for this purpose [4,12,14–18]. A thorough literature review reveals that majority of the existing surgical manipulators are based on a special kind of mechanisms called RCM mechanisms. Among these mechanisms, one DOF planar RCM mechanisms have been highly popular for MIS applications [19].

Despite of their many advantages, the planar 1DOF RCM mechanisms short fall of the number of DOFs required for MIS. This study is primarily aimed at proposing a new planar RCM mechanism to overcome the limitations of traditional 1DOF double-parallelogram RCM mechanisms. The proposed solution, with all its advantages of existing planar mechanisms, provides the two most important DOFs by virtue of its mechanical design.

In a typical MIS procedure, 4DOFs are required at the incision point, namely, *pitch*, (tool) *translation*, (tool) *roll*, and *yaw*. Also the surgical tool remains virtually hinged at the *incision point* where the only possible motions are a rotation and a translation along the center of the *incision point*. Technically, the incision point is called as the RCM [4,20] which is defined as a point around which a mechanism, or a part of that mechanism, rotates. Figure 1 shows a typical RCM mechanism called double-parallelogram RCM mechanism, first used by Hamlin and Sanderson [21] and then further explored by Taylor et al. [22,23]. When joint $O_1$ or $O_2$ is actuated, the distal link of the mechanism rotates along the virtual pivot point ($O$) shown as RCM.

For the MIS workspace requirements, measurements presented in Ref. [24] show that a region defined by a circular cone with a vertex angel of 60 deg contains 95% of the total surgical tool motions during a typical MIS procedure. This region is named as Dexterous workspace (DWS). Another conic region with an elliptical base, created by two orthogonal vertex angels of 60 deg and 90 deg, is identified as the extended Dexterous workspace (EDWS) which contains the remaining 5% of the tool motions.

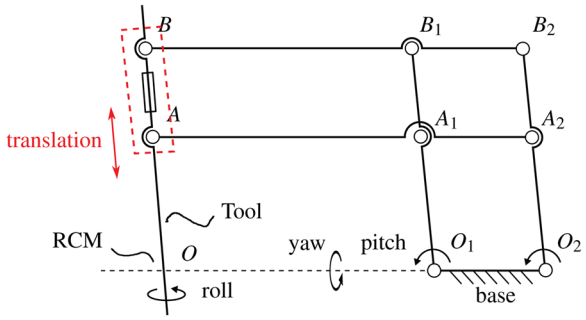


**Fig. 1 A double-parallelogram RCM mechanism**

[1]Corresponding author.

Manuscript received July 31, 2016; final manuscript received January 16, 2017; published online March 23, 2017. Assoc. Editor: Byung-Ju Yi.

  

DWS and EDWS together define the total workspace required for the MIS [25] as shown in Fig. 2.

## 2 Problem

MIS requires 4DOFs (*pitch, translation, yaw and roll*), but the existing planar RCM mechanisms, like the double-parallelogram mechanism, only provide one DOF (*pitch*). The remaining three DOFs are achieved through *external means*. For example, *yaw* is obtained by tilting the mechanism along its base link (Fig. 1), as is the case with [16,26,27]. *Roll* and *translation* are usually achieved by mounting actuators directly on the distal-end of the manipulator as suggested by van den Bedem [16] and Gijbels et al. [26]. The *roll* DOF demands less precision and is relatively easier to implement. However, the *translation* DOF when implemented using such *external means* causes several performance issues as described below.

The purpose of translation DOF is to facilitate the inward and outward movement of the surgical tool through the incision point. Traditionally, there have been two approaches to implement *translation* DOF in the planar RCM mechanisms.

**2.1 Distal-End Actuators.** In this approach, actuators are directly mounted on the distal-end of the manipulator to generate *translation* DOF. Examples of such implementation include Al-Zahrawi surgical robot [14] and SOFIE surgical system [16]. This approach offers better power transmission capabilities, but placement of actuators over distal-end makes it bulkier [4] and induces unnecessary vibrations at the tool tip. It also increases inertia of the distal-end which, consequently, increases torque and energy requirements. To avoid these issues, prismatic actuators can be a choice to implement *translation*. However, prismatic actuators are relatively expensive and affect the backdrivability of the manipulator [28].

**2.2 Cable-Pulley Scheme.** A typical example of such an implementation of *translation* DOF is da Vinci surgical robot [27]. Using this approach, actuators are installed closer to the base of manipulator and the end-effector is translated through custom-designed steel cables and pulleys. This scheme helps to achieve compact distal-end but is relatively complex to realize. It also affects the power transmission capabilities as a more significant friction factor comes into play [4]. Moreover, the cables tend to elongate after a certain period of use and require replacement. This potentially affects the operational cost and performance of the manipulator.

Given the two approaches discussed above, it is evident that the implementation of *translation* DOF through *external means* comes with a number of downsides. Therefore, it is desirable to find a solution which could provide the two most important DOFs—*pitch* and *translation*—independent of any such *external means*.

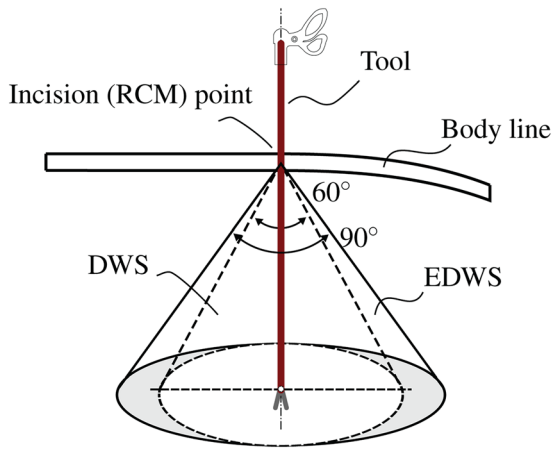


**Fig. 2 Required workspace for minimally invasive surgery**

## 3 State-of-the-Art

In the existing literature, we could find only two studies aimed at solving the limitations of 1DOF planar RCM mechanism, though indirectly. One by Li et al. [28] and another by Gijbels et al. [26]. The mechanism proposed by Li et al. provides 2DOFs—*pitch* and *translation*—and is backdrivable as well. However, owing to the link length ratios required to maintain RCM constraint, the size of the mechanism becomes larger. This increases the risk of mutual collision between the manipulators when working in close-proximity [28] such as in the case of MIS. Moreover, the weight of whole mechanism is supported by only two links and the static stability is not taken into account. A variant of this mechanism is realized and described in Ref. [29].

The mechanism proposed by Gijbels et al. also provides *pitch* and *translation* DOFs and is statically stable with actuators in energized state. However, the limited tool translation (about 30 mm) affects its suitability for MIS procedures like laparoscopy. The mechanism carries a downward protruding link toward the patient-side having a translational motion which could pose a risk of potential interference with the surgical site. It also carries a number of links toward the distal-end which are supported by a single cantilevered-link. This could induce unnecessary vibrations in the tool tip for a larger manipulator, such as intended for laparoscopic applications.

## 4 Proposed Solution

To solve the problems induced by *external means* in 1DOF RCM mechanisms and to avoid the downsides present in the existing 2DOFs RCM mechanisms, we propose a new RCM mechanism which is planar and provides the two most important DOFs by virtue of its mechanical design, i.e., without any *external means*. The mechanism design, its ability to maintain RCM constraint, kinematics, workspace, and singularities are explained below.

Based on the concept of double-parallelogram RCM mechanism, we constructed various trivial forms of the mechanism capable of providing *pitch* and *translation* DOFs. Figure 3 shows a couple of such trivial forms. These trivial forms are able to achieve RCM, but they lack in one or another aspect. For example, the mechanism shown in Fig. 3(*a*) is statically not stable which means it cannot hold its posture independently. It requires more actuators to function properly than the number of DOFs produced. Similarly, the mechanism shown in Fig. 3(*b*) is statically stable but involves many redundant links which has its own downsides for practical purposes.

If we examine these trivial mechanisms collectively, a minimalist version of the RCM mechanism can be envisaged as shown in Fig. 4. $M_1$ and $M_2$ represent the two actuators to achieve *pitch* and *translation* DOFs, while $A_3$ denotes a passive prismatic joint. If $M_1$ and $M_2$ are actuated in same direction (clockwise or counterclockwise), the mechanism generates the *pitch* motion. When both actuators are moved in opposite direction to each other, *translation* DOF is achieved. This actuation scheme makes it

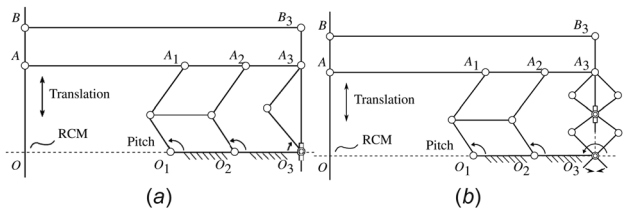


**Fig. 3 Trivial forms of the proposed two DOF RCM mechanism**

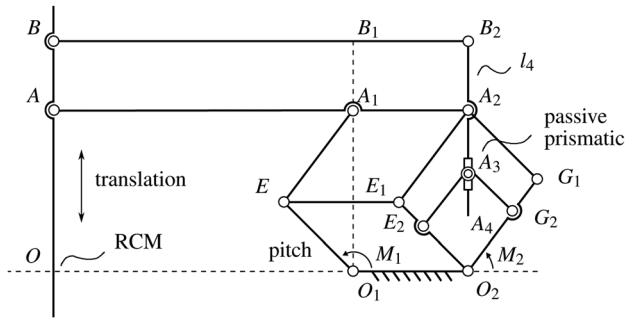


**Fig. 4 The proposed two DOF RCM mechanism**

possible to install actuators near the base of manipulator which is a desirable feature. A similar actuation scheme is used in Ref. [26].

The proposed mechanism provides the two most important DOFs without using any *external means*. It does not carry a downward protruding link contrary to the mechanism in Ref. [26]. Moreover, the number of linkages and joints in the proposed mechanism is fewer than the solution proposed in Ref. [28].

**4.1 Kinematics.** Considering the interconnected parallelograms in the mechanism, the effect of $M_1$ remains same whether it actuates link $O_1E$ or $O_2E_1$ (Fig. 4). Also to achieve RCM, segment $OA$ and $A_3B_2$ remain parallel to each other. Using these obvious conclusions, a simplified representation of the mechanism can be formed as shown in Fig. 5, where $O$ denotes the RCM point. $q_1$, $q_2$, and $q_3$ are the joint variables and $\theta$, $\phi$, and $R$ represent the *pitch*, *yaw*, and *translation* DOFs, respectively.

The position of point $A_1$ in Cartesian space can be expressed as $x = l_2\cos(q_1) + l_3\cos(q_2)$ and $y = l_2\sin(q_1) + l_3\sin(q_2)$, where $l_2$ and $l_3$ are lengths of link $O_1E$ and $EA_1$, respectively. As $\overline{OA} \parallel \overline{O_1A_1}$ and $\angle AOO_1 = \angle XO_1A_1$ are in virtual parallelogram $OO_1A_1A$, the *pitch* DOF ($\theta$) can be expressed as

$$\theta = \tan^{-1}\left(\frac{l_2\sin(q_1) + l_3\sin(q_2)}{l_2\cos(q_1) + l_3\cos(q_2)}\right) \tag{1}$$

*Translation* DOF ($R$) represents the length of distal link below the RCM point. From Fig. 5, $R = l_1 - |\overline{O_1A_1}| = l_1 - |\mathbf{r}|$, where $l_1$ is length of the distal-link. Therefore, $R$ can be expressed as

$$R = l_1 - \sqrt{l_2^2 + 2l_2l_3\cos(q_1 - q_2) + l_3^2} \tag{2}$$

*Yaw* DOF ($\phi$) is achieved by mounting actuator along the axis $OO_1$ and can be simply given by $\phi = q_3$. Based on the kinematic

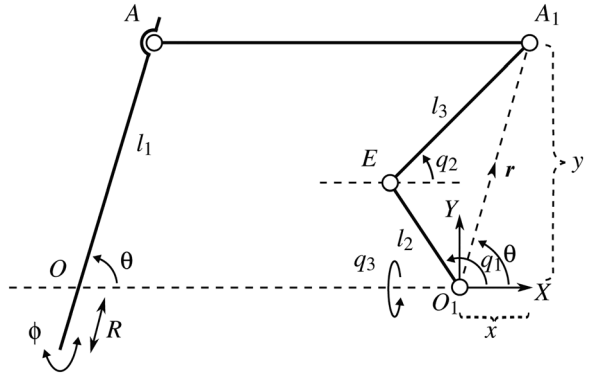


**Fig. 5 A simplified representation of the proposed RCM mechanism**

equations, a relation between the joint velocities and the distal-link tip velocities can be expressed as

$$\begin{bmatrix}\dot{R}\\ \dot{\theta}\\ \dot{\phi}\end{bmatrix} = \boldsymbol{J}(\boldsymbol{q})\begin{bmatrix}\dot{q}_1\\ \dot{q}_2\\ \dot{q}_3\end{bmatrix}, \quad \boldsymbol{J}(\boldsymbol{q}) = \begin{bmatrix}\frac{A}{\sqrt{E}} & \frac{B}{\sqrt{E}} & 0\\ \frac{C}{\sqrt{E}} & \frac{D}{\sqrt{E}} & 0\\ 0 & 0 & 1\end{bmatrix} \tag{3}$$

where a dot represents time derivative and $\boldsymbol{J}(\boldsymbol{q})$ is the Jacobian matrix with elements

$$A = l_2l_3\sin(q_1 - q_2), \quad B = -l_2l_3\sin(q_1 - q_2)$$
$$C = l_2l_3\cos(q_1 - q_2) + (l_2)^2, \quad D = l_2l_3\cos(q_1 - q_2) + (l_3)^2$$
$$E = (l_2\cos q_1 + l_3\cos q_2)^2 + (l_2\sin q_1 + l_3\sin q_2)^2$$

*4.1.1 Alignment Mechanism.* To maintain RCM in the mechanism (Fig. 4), it is vital for points $O_2, A_3, A_2, B_2$ to remain collinear with each other. It is important to note that the link $B_2A_4$ in quadrilateral $O_2E_1A_2G_1$ is not physically constrained at point $O_2$. Hence, there remains a possibility to lose the collinearity, and consequently, the RCM. To avoid this, the mechanism portion represented by quadrilateral $O_2E_1A_2G_1$ (Fig. 6), named as *alignment mechanism*, is solved to ensure collinearity.

Let us define $\boldsymbol{r}_1 = \mathbf{O_2A_2}$, $\boldsymbol{r}_2 = \mathbf{O_2A_3}$ and $l_5 = \overline{O_2G_1}$, $l_6 = \overline{O_2E_1}$, $k_5l_5 = \overline{O_2G_2}$, $k_6l_6 = \overline{O_2E_2}$, $l_{55} = \overline{G_1A_2}$, $l_{56} = \overline{E_1A_2}$, $l_{65} = \overline{G_2A_3}$, $l_{66} = \overline{E_2A_3}$, $\boldsymbol{u}_i = [\cos\theta_i \ \sin\theta_i]^{\mathrm{T}}$, $\boldsymbol{w}_{ji} = [\cos\ \theta_{ji}\ \sin\theta_{ji}]^{\mathrm{T}}$, $(i = 5, 6, j = 5, 6)$, where $\theta_i, \theta_{ii}, (i = 5, 6)$ denote the corresponding angles. A set of sufficient conditions for the collinearity of points $O_2, A_3, A_2$ is determined (See Appendix) as

$$k = k_5 = k_6, \quad (0 < k < 1) \tag{4}$$

$$k^2(l_{55}^2 - l_{56}^2) = l_{65}^2 - l_{66}^2 \tag{5}$$

To maintain geometric symmetry in the mechanism, we further assume that $l_5 = l_{56}$, $l_6 = l_{55}$, $k_5l_5 = l_{66}$, and $k_6l_6 = l_{65}$. Using $k = k_5 = k_6$, Eq. (5) holds true with these assumptions. For *alignment mechanism* (Fig. 6), the above assumptions mean that the

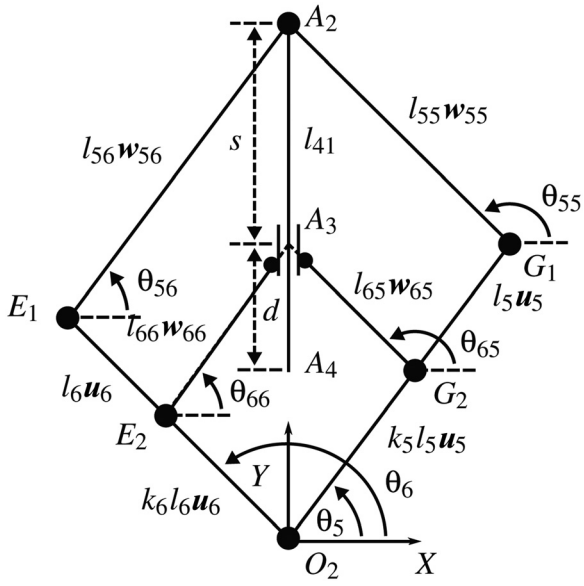


**Fig. 6 The alignment mechanism to maintain the remote center of motion constraint. $A_3$ is a passive prismatic joint.**

quadrilaterals $O_2E_1A_2G_1$ and $O_2E_2A_3G_2$ are essentially two parallelograms such that

$$\theta_5 = \theta_{56} = \theta_{66} \tag{6}$$

$$\theta_6 = \theta_{55} = \theta_{65} \tag{7}$$

After ensuring the collinearity, it is important to restrict the translational motion of link $A_2A_4$ inside the geometric boundary of the *alignment mechanism*. From Fig. 6, if $d = l_{41} - s$, where $l_{41} = |\overline{A_2A_4}|$, then $s$ can be written as $s = |\mathbf{r}_1| - |\mathbf{r}_2|$. Based on the above assumptions and their subsequent results expressed in Eqs. (6) and (7), $s$ can be further expressed as

$$s = \sqrt{l_5^2 + l_6^2 + 2l_5l_6\cos(\theta_6 - \theta_5)}$$

$$-\sqrt{k^2l_5^2 + k_6l_6^2 + 2k^2l_5l_6\cos(\theta_6 - \theta_5)} \tag{8}$$

$$s = (1-k)|\mathbf{r}_1| \tag{9}$$

Therefore, the condition to restrict motion of the link segment $l_{41}$ inside the geometric boundary of the mechanism can be determined as

$$0 < l_{41} - ((1-k)|\mathbf{r}_1|) < |\mathbf{r}_2| \tag{10}$$

**4.2 Singular Configurations.** To ascertain the suitability of the mechanism for its intended application, it is important to examine its singularities. To find singular configurations of the proposed RCM mechanism, det $\boldsymbol{J}(\boldsymbol{q})$ is solved against zero. From Eq. (3)

$$\det \boldsymbol{J}(\boldsymbol{q}) = \left| \frac{l_2l_3\sin(q_1 - q_2)}{\sqrt{l_2^2 + 2l_2l_3\cos(q_1 - q_2) + l_3^2}} \right| = 0 \tag{11}$$

This means the mechanism gets into singular configuration when $\{(q_1, q_2)|q_1 = q_2, q_1 = q_2 \pm \pi\}$. Geometrically, these singularities correspond to the mechanism configurations when parallelogram $O_1EE_1O_2$ and $EA_1A_2E_1$ become aligned or the link $O_1E$ and $EA_1$ become parallel to each other (Fig. 4).

**4.3 Optimal Configuration.** *Optimal configuration* relates to the mechanism configuration when the tip of end-effector can achieve a maximum possible velocity in any arbitrary direction from a given point inside its workspace.

For mechanisms with square Jacobian matrix, the *manipulability* is defined as $w = \det \boldsymbol{J}(\boldsymbol{q}), w \geq 0$ [30]. From Eq. (11), the manipulability measure ($w$) becomes maximum when $q_1 = q_2 + (\pi/2)$.

Geometrically, it means when links $O_1E$ and $EA_1$ will be at right angle to each otheror, in other words, when the mutual angle between the links $O_2E_1$ and $O_2G_1$ will be 90 deg (Fig. 4), the mechanism will attain its *optimal configuration*. In MIS, majority of the organs lie toward the bottom of surgical workspace. Hence, it is desirable to achieve maximum kinematic performance of the mechanism toward the bottom of its workspace.

**4.4 Mechanism Workspace.** To obtain the required workspace for MIS, we set the joint variables as $q_1 \in [\pi/4, \pi] \equiv \Omega_1$, $q_2 \in [0, 3\pi/4] \equiv \Omega_2$, and $q_3 = [-\pi/4, \pi/4] \equiv \Omega_3$, while maintaining the constraint

$$q_1 \geq q_2 + \varepsilon, \quad \varepsilon > 0 \tag{12}$$

where $\varepsilon$ is a constant to avoid singularities. Figure 7 shows a comparison of the generated workspace and the required workspace for MIS with $l_2 = l_3 = 325$ mm. It is evident that the mechanism

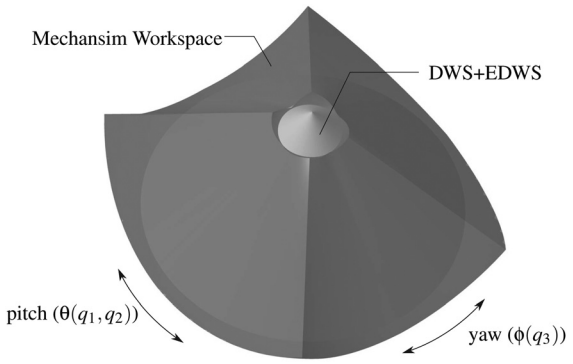


**Fig. 7 Mechanism workspace (light gray) and the required workspace for MIS (dark gray)**

can generate enough workspace to cover the surgical workspace (the sum of DWS and EDWS). Any singularities with this range of joint variables and constraint occur outside of the required workspace.

**4.5 Variant Forms of the Mechanism.** Variant forms of a mechanism provide flexibility of choice while making decision to select a suitable mechanism form for a particular application scenario. Here, we present a couple of variant forms of the proposed mechanism. From Eq. (9), it is clear that higher value of $k$ results in smaller $s$. This means in order to maximize $d$ for a given length of $l_{41}$, a higher value of $k$ is favorable ($0 < k < 1$). Based on this inference, the lengths of the rear mini-parallelogram links can be further increased as shown in Fig. 8(*a*). This results in longer *translation* DOF for the same overall size of the RCM mechanism.

Another variant form of the proposed mechanism can be achieved by implementing the *alignment mechanism* in inverted configuration as shown in Fig. 8(*b*). This results in even further reduced lengths for $l_{41}$ and the supporting links.

## 5 Mechanism Optimization

Forward kinematic equations show that the size of the mechanism workspace primarily depends on its ability to generate *pitch*, *yaw*, and *translation* DOFs. As the *yaw* DOF has one-to-one mapping, it does not require any further optimization. However, it is important to optimize the mechanism design to achieve maximum manipulability (in *pitch* direction) and tool *translation* with minimum possible link lengths. For this purpose, we define a cost function (13) which is a product of two further functions: (i) average manipulability and (ii) effective translation. Average manipulability indicates the kinematic performance of a given design candidate (pair of $\alpha, l_2$ where $\alpha = l_2/l_3$) and $r_e$ provides a measure of *translation* DOF. Here, $r_e$ acts as a sizing constraint.

In this optimization, first we maximize and analyze the effect of average manipulability (avg($w$)) and the effective translation ($r_e$) separately. Then, we maximize the overall cost function (13) so that the resulting design offers better performance on both aspects.

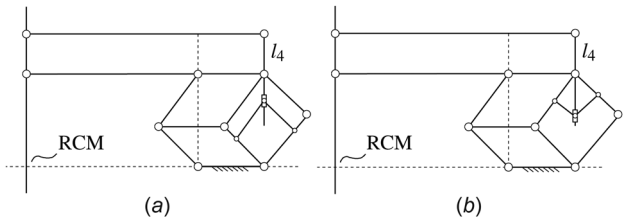


**Fig. 8 Variant forms of the proposed RCM mechanism: (*a*) offers larger translation DOF with reduced length of $l_4$, (*b*) inverted alignment mechanism can generate even larger translation with further reduced length of $l_4$**

**5.1 Problem Statement.** Find $\alpha$ and smallest $l_2$ in the proposed mechanism such that

$$\max_{l_2,\alpha}(\text{avg}(w) \times r_e) \tag{13}$$

subject to

$$(q_1, q_2) \in \Omega, \quad \Omega = \{(q_1, q_2) \in \mathbb{R}^2 : \pi/4 \le q_1 \le \pi \\ 0 \le q_2 \le 3\pi/4\} \tag{14}$$

$$\alpha = l_2/l_3, \quad (\alpha > 0) \tag{15}$$

$$q_1 \ge q_2 + \varepsilon, \quad (\varepsilon > 0) \tag{16}$$

while

$$r_{\min} \text{ covers all elements in } \Omega_4, \quad \Omega_4 = \{\theta \in \mathbb{R} : \pi/4 \le \theta \le 3\pi/4\} \tag{17}$$

In the statement above, $r_e$ denotes the effective translation of tool tip below the RCM point, avg($w$) represents the average manipulability of a mechanism design candidate, $r_{\min}$ represents the distance of point $C$ from $A$ (Fig. 11) when the mechanism is in fully retracted configuration (the end-effector is at the bottom of the workspace), and $\theta$ represents the desired range of the *pitch* DOF (Fig. 5).

Next, we evaluate both functions and develop necessary mathematics to solve the optimization problem.

**5.2 Average Manipulability (avg($w$)).** Derived from the manipulability measure [30], average manipulability function indicates the overall performance of a mechanism design candidate (pair of $l_2$, $\alpha$) in the task space. We express it as

$$\text{avg}(w) = \frac{1}{A}\int_{q_1}\int_{q_2} w(q_1, q_2)\, dq_2 dq_1 \tag{18}$$

where $w(q_1, q_2) = \det \mathrm{J}(\mathrm{q}_1, \mathrm{q}_2)$ and $A = \int_{\Omega_1}\int_{\Omega_2} dq_2 dq_1$.

*5.2.1 avg(w) Maximization.* From Eq. (15) using $\alpha = l_2/l_3$, $\alpha > 0$, the manipulability measure ($w$) in Eq. (11) for the mechanism becomes

$$w(q_1, q_2) = \left| \frac{l_2 \sin(q_1 - q_2)}{\sqrt{\alpha^2 + 2\alpha\cos(q_1 - q_2) + 1}} \right| \tag{19}$$

Using Eq. (19), the average manipulability (18) is analyzed for the following three cases:

For case:1, when $\alpha = 1$ the denominator of Eq. (19) simply reduces to $\sqrt{2(1 + \cos(q_1 - q_2))}$. For case:2, when $\alpha < 1$ the denominator in Eq. (19) becomes smaller than the denominator in case:1. For same numerator, a smaller denominator in case:2 means the resultant avg($w$) in case:2 is bigger than the avg($w$) in case:1.

Similarly for case:3, when $\alpha > 1$, it is obvious that the denominator in Eq. (19) becomes bigger than the one in case:1. For same numerator, bigger denominator means the resultant avg($w$) in case:3 is smaller than the avg($w$) in case:1. This means the avg($w$) in case:2 is bigger than the one in case:1 and the avg($w$) in case:3 is smaller than that of the case:1. This implies that the avg($w$) in case:2 is also bigger than the avg($w$) in case:3. In other words, for any values of $l_2$, $l_3$ and given range of $q_1$, $q_2$, $w$ will be maximum for case:2 only.

The above analytical findings are also verified through numerical simulation. The plot in Fig. 9 demonstrates that for any $l_2$, the measure avg($w$) tends to maximize when $\alpha$ is less than one. This means that smaller $\alpha$ yields higher average manipulability for the mechanism. Also, it suggests that longer $l_2$ outputs higher average manipulability.

Therefore, it is concluded that the kinematic performance of the mechanism gets maximized for case:2

$$\alpha < 1 \quad \text{or} \quad l_2 < l_3 \tag{20}$$

The above conclusion has certain impact on the physical form of the mechanism. Figure 10 represents the corresponding mechanism forms for all three cases of $\alpha$. For any given values of $l_2$ and $l_3$, average manipulability measure (avg($w$)) is maximum for the form ($a$) shown in Fig. 10.

**5.3 Effective Translation ($r_e$).** Effective translation represents the effective range of tool tip *translation* required for surgical purposes. In the simplified representation shown in Fig. 11, it is the distance traveled by point $C$ on the line $AC$, denoted as $r_e$. It can be computed as $r_e = r_{\max} - r_{\min}$. Here, $r_{\max}$ represents the distance of point $C$ from $A$ when the mechanism is in fully extended configuration. In this situation, the corresponding angle $q_1$ is denoted as $q_1'$ and $q_2$ as $q_2'$. Similarly, $r_{\min}$ represents the distance of $C$ from $A$ when the mechanism is in fully retracted configuration, i.e., the end-effector tip is at the bottom of the mechanism workspace. In this situation, the corresponding angle $q_1$ is denoted as $q_1''$ and $q_2$ as $q_2''$. The limit of mechanism extension ($r_{\max}$) is dictated by its geometric design, i.e., avoiding singularities, whereas the limit of retracted configuration is defined by the range of desired pitch angles expressed in Eq. (17).

From Fig. 11, $r_e$ can be expressed as

$$r_e = l_2 \sin(q_1') + l_3 \sin(q_2') - l_2 \sin(q_1'') \\ -l_3 \sin(q_2'') \tag{21}$$

If we assume $l_2 = \alpha l_3$, Fig. 12 shows the possible retracted configurations of the mechanism when $\theta = \pi/2$. From Fig. 12, it is clear that the mechanism will satisfy constraint (17)—achieve the desired pitch region—if the following two conditions hold true:

$$q_1 < 3\pi/4 \tag{22}$$

$$q_2 > \pi/4 \tag{23}$$

If Eqs. (22) and (23) do not hold, the range of pitch motion of the mechanism becomes smaller than the desired pitch range as the mechanism reaches its limit without satisfying Eq. (17). Therefore, the result of $r_e$ maximization for a design candidate

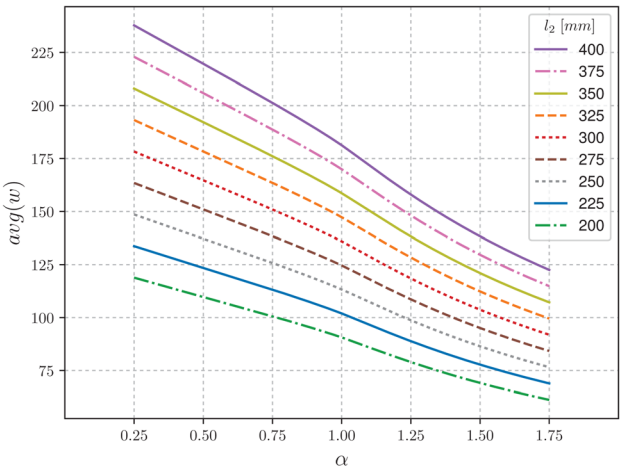


**Fig. 9 Average manipulability over the range of $\alpha$ ($\alpha = l_2/l_3, \alpha > 0$)**

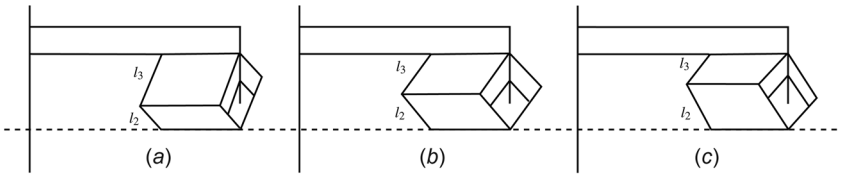


**Fig. 10 Corresponding mechanism forms for cases of $\alpha$ ($\alpha = l_2/l_3$): (*a*) $\alpha < 1$, (*b*) $\alpha = 1$, and (*c*) $\alpha > 1$**

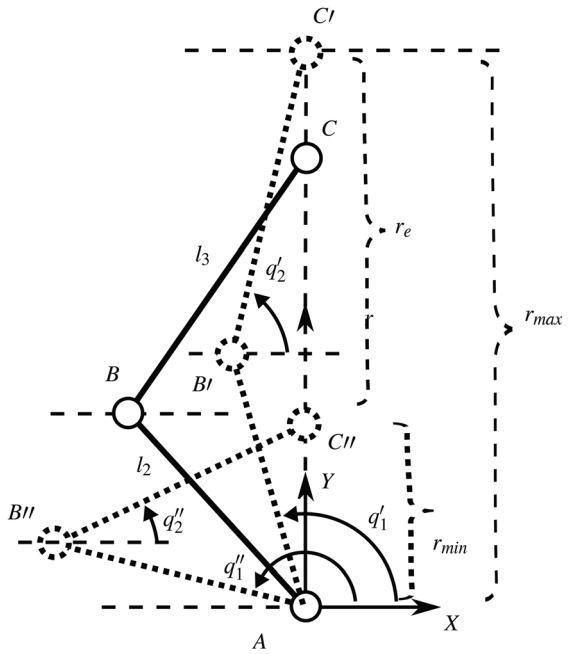


**Fig. 11 Effective translation in the simplified representation of the proposed mechanism**

satisfying Eqs. (22) and (23) when $\theta = \pi/2$ can be generalized for any value of $\theta$ in the desired *pitch* range defined in Eq. (17). This reduces the problem complexity and computational load significantly. In Fig. 12, only cases (*a*), (*b*), and (*e*) satisfy the conditions (22) and (23). As (*c*) and (*d*) do not satisfy Eqs. (22) and (23), they are excluded from further optimization.

Now for case (*a*), it is easy to visualize that $q_1$ and $q_2$ have equal range of motion (both joints will move equally when the mechanism gets in to fully extended configuration). For case (*b*), $q_1$ has larger range of motion than $q_2$ as $q_2$ will reach to $\pi/2$ from its current position more quickly than $q_1$, while the mechanism achieves fully extended configuration. On similar lines, $q_2$ has larger range of motion than $q_1$ for case (*e*). Therefore, for cases (*a*) and (*b*), we calculate $q_2$ for any given $q_1$, and for case (*e*), we calculate $q_1$ for any given $q_2$.

From Fig. 12(*a*), the parallelogram *OADB* can be expressed in terms of two triangles: $\Delta OAD$ and $\Delta OBD$. $\Delta OAD$ can be further divided into two right-angle triangles $\Delta OAC$ and $\Delta ACD$. From $\Delta OAC$

$$a = l_2 \sin(q_1 - \pi/2) \tag{24}$$

and from $\Delta ACD$

$$q_2 = \cos^{-1}\left(\frac{a\alpha}{l_2}\right) \tag{25}$$

Substituting $a$ from Eq. (24)

$$q_2 = \cos^{-1}(\alpha \sin(q_1 - \pi/2)) \tag{26}$$

Therefore, $q_2'$ and $q''_2$ can be expressed as

$$q_2' = \cos^{-1}(\alpha \sin(q''_1 - \pi/2) \tag{27}$$

$$q''_2 = \cos^{-1}(\alpha \sin(q_1' - \pi/2)) \tag{28}$$

For case (*e*), we express $q_1$ in terms of $q_2$. From Eq. (26), $q_1$ can be calculated as

$$q_1 = \sin^{-1}(\cos(q_2)/\alpha) + \pi/2 \tag{29}$$

Therefore, $q_1'$ and $q''_1$ can be expressed as

$$q_1' = \sin^{-1}(\cos(q''_2)/\alpha) + \pi/2 \tag{30}$$

$$q''_1 = \sin^{-1}(\cos(q_2')/\alpha) + \pi/2 \tag{31}$$

*5.3.1 $r_e$ Maximization.* After the necessary formulation, we now maximize $r_e$ with $l_2$ and $\alpha$ as tuning parameters. For case:1 and case:2 ($\alpha \leq 1$, Figs. 12(*a*) and 12(*b*)), $r_e$ is evaluated by using $q_2'$ and $q''_2$ as derived in Eqs. (27) and (28). Similarly, for case:3

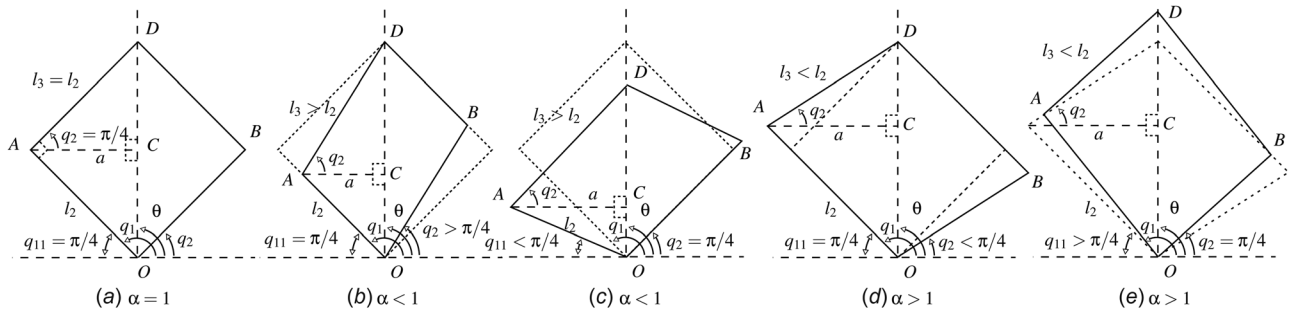


**Fig. 12 Rear-parallelogram configurations for cases $\alpha = 1$, $\alpha < 1$ and $\alpha > 1$ when $\theta = \pi/2$. Distance *OD* represents $r_{min}$. Only case (*a*), (*b*), and (*e*) can generate the desired workspace ($\pi/4 \leq \theta \leq 3\pi/4$) as they satisfy the constraint (22) and (23). As (*c*) and (*d*) do not satisfy Eqs. (22) and (23), they are excluded from $r_e$ optimization.**

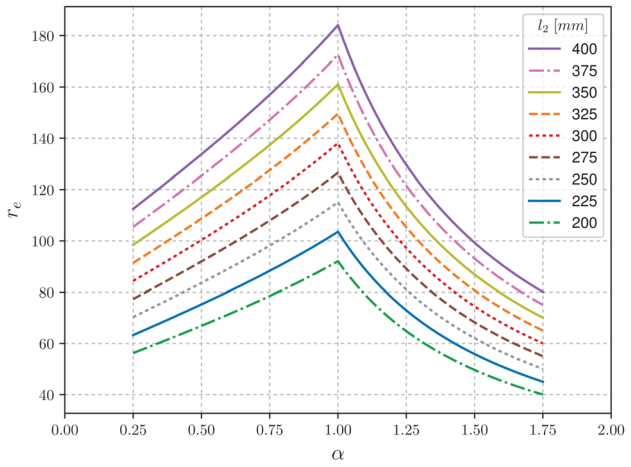


**Fig. 13 Effective translation over the range of $\alpha$ ($\alpha = l_2/l_3$, $\alpha > 0$)**

($\alpha > 1$, Fig. 12(*e*)), $r_e$ is evaluated by using $q_1'$ and $q_1''$ as derived in Eqs. (30) and (31), respectively.

The plot shown in Fig. 13 demonstrates that for all values of $l_2$ effective translation $r_e$ tends to maximize when $\alpha$ is equal to one. Similar to the average manipulability function, longer link length of $l_2$ returns higher value of $r_e$. Therefore, we conclude that for any corresponding values of $l_2$ and $\alpha$ in the given range, $r_e$ favors case:1

$$\alpha = 1 \quad \text{or} \quad l_2 = l_3 \tag{32}$$

Like the average manipulability maximization, the above conclusion also has certain impact on the physical form of the mechanism. Figure 10 represents the corresponding mechanism forms for all three cases of $\alpha$. For any given values of $l_2$ and $\alpha$, effective translation ($r_e$) becomes maximum for the form (*b*).

**5.4 Optimal Design.** We now maximize the overall cost function (13) which is product of the average manipulability function and the effective translation of the mechanism. The plot in Fig. 14 demonstrates that the overall cost function maximizes for case:1. Therefore, for any corresponding values of $l_2$ and $\alpha$ in the given range, the optimal design corresponds to the case:1

$$\alpha = 1 \quad \text{or} \quad l_2 = l_3 \tag{33}$$

Consequently, the optimum link lengths can be calculated by considering case:1. By substitute $r_e$ in Eq. (21) with desired effective translation ($r_{ed}$) and using $\alpha = 1$, we can calculate $l_2$ and $l_3$.

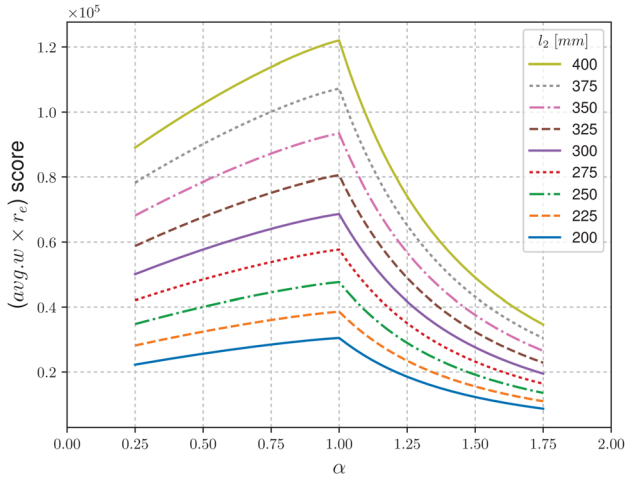


**Fig. 14 Combined performance score over the range of $\alpha$ ($\alpha = l_2/l_3, \alpha > 0$)**

Similarly, substituting $R$ with desired effective translation ($r_{ed}$) and $r$ with $r_{min}$ in Eq. (2), $l_1$ can be determined to achieve the required workspace for MIS.

## 6 Conclusion

To solve the problems of existing 1DOF RCM mechanisms, a new 2DOFs planar RCM mechanism is proposed. The proposed design provides *pitch* and *translation* DOF without using any external means such as cable-pulleys or actuators mounted directly on the distal-end of the manipulator. The mechanism satisfies the MIS workspace requirements and an *optimal configuration* is selected such that the maximum kinematic performance is achieved toward the bottom of the workspace.

The design optimization shows that the maximum kinematic performance of the mechanism is achieved when the adjacent parallelograms have same lengths for the vertical links ($\alpha = 1$). It ensures that the maximum manipulability and the desired translational motion of the end-effector is achieved with a minimum possible size of the mechanism.

Moreover, the proposed mechanism design does not include any active prismatic joints which makes it ideal for a fully backdrivable manipulator implementation. The geometric design of the mechanism is simpler than the existing 2DOFs RCM mechanisms described in the state-of-the-art. It uses fewer number of links and joints than the mechanism proposed in Ref. [28]. Contrary to the solution in Ref. [26], the absence of protruding links minimizes chances of any untoward interference with the surgical site. Unlike Ref. [26], there is no cantilevered-link as the main part of this mechanism which results in a more rigid and stiffer design for practical applications.

The ability to achieve *translation* DOF without external means makes distal-end of the mechanism compact and slender. This is highly desirable in surgical applications where multiple robotic manipulators are supposed to work in close proximity. The compact distal-end makes it particularly suitable for surgeries where the tool is supposed to maneuver in confined and narrow spaces such as laparoscopy and retinal MIS. The mechanism is a potential choice for manipulator designs aimed at achieving high backdrivability, low design complexity, compact distal-ends, and higher power transmission capabilities.

As a future work, we plan to consider the force transmission efficiency of the mechanism for better dynamic performance and develop a surgical manipulator for MIS applications.

## Appendix: Conditions of Collinearity for Alignment Mechanism

In *alignment mechanism* (Fig. 6), let us define $\mathbf{r}_1$ and $\mathbf{r}_2$ as the position vectors of points $A_2$ and $A_3$ with respect to $O_2$ and their closed-loop equations can be written as

$$\boldsymbol{r}_1 = l_i \boldsymbol{u}_i + l_{5i} \boldsymbol{w}_{5i}, \quad \boldsymbol{r}_2 = k_i l_i \boldsymbol{u}_i + l_{6i} \boldsymbol{w}_{6i} \tag{A1}$$

where $i = 5, 6$ $(0 < k < 1)$ and $\boldsymbol{u}_i$, $\boldsymbol{w}_{5i}$, $\boldsymbol{w}_{6i}$ are the respective direction vectors. The Cartesian position of $A_2$ and $A_3$ in $XY$-plane can be expressed as

$$\boldsymbol{r}_1 = [x_{A2} \quad y_{A2}]^{\mathrm{T}} \tag{A2}$$

$$\boldsymbol{r}_2 = [x_{A3} \quad y_{A3}]^{\mathrm{T}} \tag{A3}$$

and

$$\boldsymbol{u}_i = [\cos\theta_{5i} \quad \sin\theta_{5i}]^{\mathrm{T}}, \quad \boldsymbol{w}_{5i} = [\cos\theta_{5i} \quad \sin\theta_{5i}]^{\mathrm{T}}$$
$$\boldsymbol{w}_{6i} = [\cos\theta_{6i} \quad \sin\theta_{6i}]^{\mathrm{T}}$$

If we assume $\mathbf{r}_1$ and $\mathbf{r}_2$ as collinear vectors, then their relationship can be expressed as $\mathbf{r}_1 = \lambda \mathbf{r}_2$, where $\lambda$ is a scalar multiple with value greater than one. Above relation can also be written as

$$\begin{bmatrix} x_{A2} \\ y_{A2} \end{bmatrix} = \lambda \begin{bmatrix} x_{A3} \\ y_{A3} \end{bmatrix} \tag{A4}$$

If $x_{A2} = \lambda x_{A3}$ and $\lambda = y_{A2}/y_{A3}$, Eq. (A4) can be expressed in terms of the ratios of the Cartesian coordinates of $A_2$ and $A_3$

$$x_{A2} : y_{A2} = x_{A3} : y_{A3} \tag{A5}$$

Equation (A5) represents the necessary and sufficient condition of collinearity for $\mathbf{r}_1$ and $\mathbf{r}_2$. In order to find the above ratios, we rearrange and take norm of Eq. (A1)

$$\boldsymbol{r}_1^{\mathrm{T}}\boldsymbol{r}_1 + l_i^2 - 2l_i\boldsymbol{r}_1^{\mathrm{T}}\boldsymbol{u}_i = l_{5i}^2 \tag{A6}$$

$$\boldsymbol{r}_2^{\mathrm{T}}\boldsymbol{r}_2 + (k_i l_i)^2 - 2k_i l_i \boldsymbol{r}_2^{\mathrm{T}}\boldsymbol{u}_i = l_{6i}^2 \tag{A7}$$

where $i = 5, 6$. Substituting expressions for $\boldsymbol{r}_1, \boldsymbol{r}_2, \boldsymbol{u}_i, \boldsymbol{w}_{5i}$, and $\boldsymbol{w}_{6i}$ in above pair of equations

$$2l_i \cos\theta_i x_{A2} + 2l_i \sin\theta_i y_{A2} + \left(l_{5i}^2 - l_i^2 - x_{A2}^2 - y_{A2}^2\right) = 0 \tag{A8}$$

$$2k_i l_i \cos\theta_i x_{A3} + 2k_i l_i \sin\theta_i y_{A3} + \left(l_{6i}^2 - k_i^2 l_i^2 - x_{A3}^2 - y_{A3}^2\right) = 0 \tag{A9}$$

Equation (A8) represents two equations as $i = 5, 6$. Same is the case with Eq. (A9). Solving both equations individually for $i = 5, 6$ results in

$$2(l_5 \cos\theta_5 - l_6 \cos\theta_6)x_{A2} + 2(l_5 \sin\theta_5 - l_6 \sin\theta_6)y_{A2} + \left(l_6^2 - l_5^2 + l_{55}^2 - l_{56}^2\right) = 0 \tag{A10}$$

$$2(k_5 l_5 \cos\theta_5 - k_6 l_6 \cos\theta_6)x_{A3} + 2(k_5 l_5 \sin\theta_5 - k_6 l_6 \sin\theta_6)y_{A3} + \left(l_{65}^2 - l_{66}^2 + k_6^2 l_6^2 - k_5^2 l_5^2\right) = 0 \tag{A11}$$

Equations (A10) and (A11) represent the position of point $A_2$ and $A_3$ in terms of related link lengths and joint angles. Using both equations, the ratios of respective coordinates can be expressed as

$$\frac{x_{A2}}{y_{A2}} = \frac{l_5^2 - l_6^2 + l_{56}^2 - l_{55}^2 - 2(l_5 \sin\theta_5 - l_6 \sin\theta_6)y_{A2}}{2(l_5 \cos\theta_5 - l_6 \cos\theta_6)y_{A2}} \tag{A12}$$

$$\frac{x_{A3}}{y_{A3}} = \frac{k_5^2 l_5^2 - k_6^2 l_6^2 + l_{66}^2 - l_{65}^2 - 2(k_5 l_5 \sin\theta_5 - k_6 l_6 \sin\theta_6)y_{A3}}{2(k_5 l_5 \cos\theta_5 - k_6 l_6 \cos\theta_6)y_{A3}} \tag{A13}$$

From Eqs. (A12) and (A13), the conditions for which Eq. (A5) holds true can be written as

$$l_5^2 - l_6^2 = l_{55}^2 - l_{56}^2 \tag{A14}$$

$$k_5^2 l_5^2 - k_6^2 l_6^2 = l_{65}^2 - l_{66}^2 \tag{A15}$$

$$\frac{l_5 \sin\theta_5 - l_6 \sin\theta_6}{l_5 \cos\theta_5 - l_6 \cos\theta_6} = \frac{k_5 l_5 \sin\theta_5 - k_6 l_6 \sin\theta_6}{k_5 l_5 \cos\theta_5 - k_6 l_6 \cos\theta_6} \tag{A16}$$

If we suppose $l_5 \sin\theta_5 = a$, $l_6 \sin\theta_6 = b$, $l_5 \cos\theta_5 = c$, and $l_6 \cos\theta_6 = d$, the condition to satisfy Eq. (A16) can be calculated from

$$\frac{a-b}{c-d} = \frac{k_5 a - k_6 b}{k_5 c - k_6 d} \tag{A17}$$

which is $k_5 = k_6$. Considering

$$k_5 = k_6 = k \tag{A18}$$

and using Eqs. (A15) and (A14), we can express

$$k^2\left(l_{55}^2 - l_{56}^2\right) = l_{65}^2 - l_{66}^2 \tag{A19}$$

Therefore, Eqs. (A18) and (A19) represent a pair of sufficient conditions to make points $A_2$ and $A_3$ collinear independent of the pose of the mechanism. A similar conclusion for a slightly different mechanism form is presented in Ref. [28].

## References


[1] Hawks, J. A., Kunowski, J., and Platt, S. R., 2012, "In Vivo Demonstration of Surgical Task Assistance Using Miniature Robots," IEEE Trans. Biomed. Eng., **59**(10), pp. 2866–2873.

[2] Hu, J. C., Gu, X., Lipsitz, S. R., Barry, M. J., D'Amico, A. V., Weinberg, A. C., and Keating, N. L., 2009, "Comparative Effectiveness of Minimally Invasive vs Open Radical Prostatectomy," JAMA, **302**(14), pp. 1557–1564.

[3] Verhage, R., Hazebroek, E., Boone, J., and Van Hillegersberg, R., 2009, "Minimally Invasive Surgery Compared to Open Procedures in Esophagectomy for Cancer: A Systematic Review of the Literature," Minerva Chir., **64**(2), pp. 135–146.

[4] Nisar, S., and Hasan, O., 2015, "Telesurgical Robotics," *Encyclopedia of Information Science and Technology*, GI Global, Hershey, PA, pp. 5482–5490.

[5] Tinelli, R., Litta, P., Meir, Y., Surico, D., Leo, L., Fusco, A., Angioni, S., and Cicinelli, E., 2014, "Advantages of Laparoscopy Versus Laparotomy in Extremely Obese Women (BMI > 35) With Early-Stage Endometrial Cancer: A Multicenter Study," Anticancer Res., **34**(5), pp. 2497–2502.

[6] Peters, J. H., Gibbons, G., Innes, J., Nichols, K., Roby, S., and Ellison, E., 1991, "Complications of Laparoscopic Cholecystectomy," Surgery, **110**(4), pp. 769–777.

[7] Yau, K. K., Siu, W. T., Tang, C. N., Yang, G. P. C., and Li, M. K. W., 2007, "Laparoscopic Versus Open Appendectomy for Complicated Appendicitis," J. Am. Coll. Surg., **205**(1), pp. 60–65.

[8] Berguer, R., Smith, W., and Chung, Y., 2001, "Performing Laparoscopic Surgery Is Significantly More Stressful for the Surgeon Than Open Surgery," Surg. Endoscopy, **15**(10), pp. 1204–1207.

[9] Vitiello, V., Lee, S., Cundy, T. P., and Yang, G. Z., 2013, "Emerging Robotic Platforms for Minimally Invasive Surgery," IEEE Rev. Biomed. Eng., **6**, pp. 111–126.

[10] Basdogan, C., De, S., Kim, J., Muniyandi, M., Kim, H., and Srinivasan, M., 2004, "Haptics in Minimally Invasive Surgical Simulation and Training," IEEE Comput. Graphics Appl., **24**(2), pp. 56–64.

[11] Dankelman, J., 2004, "Surgical Robots and Other Training Tools in Minimally Invasive Surgery," IEEE International Conference on Systems, Man and Cybernetics (SMC), Hague, The Netherlands, Oct. 10–13, Vol. 3, pp. 2459–2464.

[12] Kuo, C. H., and Dai, J. S., 2009, "Robotics for Minimally Invasive Surgery: A Historical Review From the Perspective of Kinematics," International Symposium on History of Machines and Mechanisms, Springer Science & Business Media, Dordrecht, The Netherlands, pp. 337–354.

[13] Dakin, G., and Gagner, M., 2003, "Comparison of Laparoscopic Skills Performance Between Standard Instruments and Two Surgical Robotic Systems," Surg. Endoscopy Other Interventional Tech., **17**(4), pp. 574–579.

[14] Hassan, T., Hameed, A., Nisar, S., Kamal, N., and Hasan, O., 2014, "Al-Zahrawi: A Telesurgical Robotic System for Minimal Invasive Surgery," IEEE Syst. J., **10**(99), pp. 1–11.

[15] Madhani, A. J., and Salisbury, J. K., 1998, "Force-Reflecting Surgical Instrument and Positioning Mechanism for Performing Minimally Invasive Surgery With Enhanced Dexterity and Sensitivity," U.S. Patent No. 5,807,377.

[16] van den Bedem, L., 2010, "Realization of a Demonstrator Slave for Robotic Minimally Invasive Surgery," Ph.D. thesis, Department of Mechanical Engineering, Technische Universiteit Eindhoven, Eindhoven, The Netherlands.

[17] Hannaford, B., Rosen, J., Friedman, D. W., King, H., Roan, P., Cheng, L., Glozman, D., Ma, J., Kosari, S. N., and White, L., 2013, "Raven-II: An Open Platform for Surgical Robotics Research," IEEE Trans. Biomed. Eng., **60**(4), pp. 954–959.

[18] Sung, G. T., and Gill, I. S., 2001, "Robotic Laparoscopic Surgery: A Comparison of the da Vinci and Zeus Systems," Urology, **58**(6), pp. 893–898.

[19] Zong, G., Pei, X., Yu, J., and Bi, S., 2008, "Classification and Type Synthesis of 1-DOF Remote Center of Motion Mechanisms," Mech. Mach. Theory, **43**(12), pp. 1585–1595.

[20] Aksungur, S., 2015, "Remote Center of Motion (RCM) Mechanisms for Surgical Operations," Int. J. Appl. Math., Electron. Comput., **3**(2), pp. 119–126.

[21] Hamlin, G., and Sanderson, A., 1994, "A Novel Concentric Multilink Spherical Joint With Parallel Robotics Applications," IEEE International Conference on Robotics and Automation (ICRA), San Diego, CA, May 8–13, Vol. 2, pp. 1267–1272.

[22] Taylor, R., Funda, J., Eldridge, B., Gomory, S., Gruben, K., LaRose, D., Talamini, M., Kavoussi, L., and Anderson, J., 1995, "A Telerobotic Assistant for Laparoscopic Surgery," IEEE Eng. Med. Biol. Mag., **14**(3), pp. 279–288.

[23] Taylor, R., Funda, J., Grossman, D., Karidis, J., and LaRose, D., 1995, "Remote Center-of-Motion Robot for Surgery," U.S. Patent No. 5,397,323.

[24] Rosen, J., Brown, J., Chang, L., Barreca, M., Sinanan, M., and Hannaford, B., 2002, "The Bluedragon—A System for Measuring the Kinematics and Dynamics of Minimally Invasive Surgical Tools In-Vivo," IEEE International Conference on Robotics and Automation (ICRA), Washington, DC, May 11–15, Vol. 2, pp. 1876–1881.

[25] Lum, M., Rosen, J., Sinanan, M., and Hannaford, B., 2006, "Optimization of a Spherical Mechanism for a Minimally Invasive Surgical Robot: Theoretical and Experimental Approaches," IEEE Trans. Biomed. Eng., **53**(7), pp. 1440–1445.
[26] Gijbels, A., Wouters, N., Stalmans, P., Van Brussel, H., Reynaerts, D., and Poorten, E. V., 2013, "Design and Realisation of a Novel Robotic Manipulator for Retinal Surgery," IEEE/RSJ International Conference on Intelligent Robots and Systems (IROS), Tokyo, Japan, Nov. 3–7, pp. 3598–3603.
[27] Devengenzo, R., Solomon, T., and Cooper, T., 2015, "Cable Tensioning in a Robotic Surgical System," U.S. Patent No. 9,050,119.
[28] Li, J., Zhang, G., Xing, Y., Liu, H., and Wang, S., 2014, "A Class of 2-Degree-of-Freedom Planar Remote Center-of-Motion Mechanisms Based on Virtual Parallelograms," ASME J. Mech. Rob., **6**(3), p. 031014.
[29] Kong, K., Li, J., Zhang, H., Li, J., and Wang, S., 2016, "Kinematic Design of a Generalized Double Parallelogram Based RCM Mechanism for Minimally Invasive Surgical Robot," ASME J. Med. Devices, **10**(4), p. 041006.
[30] Yoshikawa, T., 1985, "Manipulability of Robotic Mechanisms," Int. J. Rob. Res., **4**(2), pp. 3–9.